BMP-3 and BMP-6 Structures Illuminate the Nature of Binding Specificity with Receptors[†,‡]

George P. Allendorph,[§,||] Michael J. Isaacs,[§,⊥] Yasuhiko Kawakami,[@] Juan Carlos Izpisua Belmonte,[@,¥] and Senyon Choe*[,§,⊥]

Structural Biology Laboratory and Gene Expression Laboratory, Salk Institute for Biology Studies, 10010 North Torrey Pines Road, La Jolla, California 92037, Department of Chemistry and Biochemistry and Divison of Biological Sciences, University of California, San Diego, 9500 Gilman Drive, La Jolla, California 92037, and Center for Regenerative Medicine in Barcelona, Dr. Aiguader, 88, 08003 Barcelona, Spain

Received May 11, 2007; Revised Manuscript Received August 30, 2007

ABSTRACT: Bone morphogenetic proteins (BMPs) are extracellular messenger ligands involved in controlling a wide array of developmental and intercellular signaling processes. To initiate their specific intracellular signaling pathways, the ligands recognize and bind two structurally related serine/threonine kinase receptors, termed type I and type II, on the cell surface. Here, we present the crystal structures of BMP-3 and BMP-6, of which BMP-3 has remained poorly understood with respect to its receptor identity, affinity, and specificity. Using surface plasmon resonance (BIAcore) we show that BMP-3 binds Activin Receptor type II (ActRII) with $K_d \approx 1.8$ μM but ActRIIb with 30-fold higher affinity at $K_d \approx 53$ nM. This low affinity for ActRII may involve Ser-28 and Asp-33 of BMP-3, which are found only in BMP-3's type II receptor-binding interfaces. Point mutations of either residue to alanine results in up to 20-fold higher affinity to either receptor. We further demonstrate by Smad-based whole cell luciferase assays that the increased affinity of BMP-3_{S28A} to ActRII enables the ligand's signaling ability to a level comparable to that of BMP-6. Focusing on BMP-3's preference for ActRIIb, we find that Lys-76 of ActRII and the structurally equivalent Glu-76 of ActRIIb are distinct between the two receptors. We demonstrate that $ActRIIb_{E76K}$ and ActRII bind BMP-3 with similar affinity, indicating BMP-3 receptor specificity is controlled by the interaction of Lys-30 of BMP-3 with Glu-76 of ActRIIb. These studies illustrate how a single amino acid can regulate the specificity of ligand−receptor binding and potentially alter biological signaling and function in vivo.

Transforming growth factor beta (TGF-β)[1] superfamily ligands are extracellular messengers that signal through specific interactions with receptors on the surface of target cells. Approximately 40 members of the superfamily are found in the human genome and can be divided into several functional subfamilies including TGF-β, bone morphogenetic protein (BMP), growth and differentiation factor (GDF), activin and inhibin, and mullerian inhibiting substance (MIS). These ligands are involved in a diverse range of cellular processes from dorsal/ventral patterning to bone formation and tissue repair to cell proliferation and differentiation (*1*). Therefore, modulation of specific ligand−receptor interactions can be an effective therapeutic means to control a variety of diseases ranging from skeletal and muscle abnormalities to metabolic disorders and neoplastic developments (*2*, *3*). In recent years, TGF-β ligands have been shown to be critical ingredients in the maintenance and guidance of stem cell differentiation and tissue regeneration (*4*, *5*).

The hallmark feature of TGF-β superfamily ligands is their conserved structural architecture that provides an underlying basis for the varying degrees of overlapping specificity seen among ligand−receptor pairs. TGF-β ligands are synthesized as inactive precursor molecules composed of an N-terminal prodomain and a C-terminal mature domain. To become functional, the mature domain must first be cleaved from the prodomain by a protease such as furin (*6*). Each mature ligand subunit contains a unique scaffold consisting of three disulfide bonds arranged in what is known as the 'cystine knot' motif (*7*). Connecting two mature subunits is an intersubunit disulfide bond, generating the biologically active form, a covalently linked dimer. The characteristic fold of each subunit includes four beta strands forming two fingers, giving the dimer a general appearance of a butterfly with

[†] This work was supported by grants from the National Institutes of Health HD013527 (S.C.), CIRM (S.C.), HD042167 (J.C.I.B.), the G. Harold and Leila Y. Mathers Charitable Foundation (J.C.I.B.), and the Chapman Foundation Fellowship (G.P.A.).

[‡] The coordinates of BMP-3 and BMP-6 have been deposited in the RCSB Protein Data Bank (PDB id 2QCQ and 2QCW for BMP-3 and BMP-6, respectively).

* To whom correspondence should be addressed. Phone: (858) 453-4100. Fax: (858) 452-3683. E-mail: choe@salk.edu.

[§] Structural Biology Laboratory, Salk Institute for Biology Studies.

[@] Gene Expression Laboratory, Salk Institute for Biology Studies.

[||] Department of Chemistry and Biochemistry, University of California, San Diego.

[⊥] Divison of Biological Sciences, University of California, San Diego.

[¥] Center for Regenerative Medicine in Barcelona.

[1] Abbreviations: TGF-β, transforming growth factor beta; BMP, bone morphogenetic protein; GDF, growth and differentiation factor; ActRII, activin receptor type II; BMPRIa, bone morphogenetic protein receptor Ia; ALK, activin receptor-like kinase; ECD, extracellular domain; H3, α-helix 3; FBS, fetal bovine serum.

10.1021/bi700907k CCC: $37.00
Published on Web 10/09/2007

the 'cystine knot' as the body and the two fingers as wings spreading from the body. Some ligands, such as GDF-9 and BMP-15, lack the cysteine forming the inter-subunit disulfide bond yet still form stable dimers (*8*). TGF-β superfamily dimers have been found to exist mostly as homodimers but also as heterodimers *in vivo* (*9*, *10*).

The ligand-specific signaling process at the target cell initiates when the TGF-β ligand recruits two each of two receptor sets, termed type I and type II. To date, seven type I and five type II receptors have been identified in the human genome. The receptors possess an extracellular domain (ECD) arranged in the three-finger toxin fold (*11*), a single transmembrane domain, and a large intracellular serine/threonine kinase domain. The ligands are known to bind the receptors in a sequential manner, first to the high-affinity receptors and then to the lower affinity receptors. In general, the high-affinity receptors are the type II receptors, but some ligands, such as BMP-2 and GDF-5, possess higher affinity for their type I receptors (*12*). The structural basis of this sequential binding has been partially explained by a membrane-restricted conformational change of the flexible ligand, as illustrated by the 'wing-spread hypothesis' for activin (*13*) during the process of forming the 2-fold-symmetric assembly of ligand and both receptor sets (*14*). This model may apply to a different mode of assembly of other flexible ligands, such as TGF-βIII (*15*). However, the hypothesis predicts that ligand flexibility will not affect the mode of assembly for rigid ligands such as the BMP subfamily. There is evidence indicating that only when all four receptors are assembled with the dimeric ligand, in a 6-member ternary complex, can the downstream signaling cascade begin (*16*). The constitutively active type II receptors phosphorylate the type I receptors, which in turn phosphorylate the intracellular Smad molecules. These phosphorylated Smads translocate to the nucleus and interact with transcriptional regulators (*17*, *18*). Additionally, the signaling cascade initiated by the ligand-specific receptor assembly is modulated locally by the presence of 'extracellular' antagonists (e.g., Noggin and inhibin), 'intramembrane' pseudo-receptors lacking an intracellular kinase domain (e.g., BAMBI), or 'intracellular' inhibitory Smads (e.g., Smad-7) (*18*, *19*).

The BMP subfamily was originally discovered by its ability to induce ectopic bone growth in mammals (*20*), but subsequent studies have shown that BMP ligands are involved in a much wider range of cellular functions (*1*−*3*, *21*). Members of the BMP family generally have the ability to bind a wide range of receptors. While activins are able to bind ActRIb (ALK-4), ActRII, and ActRIIb, BMPs are able to bind BMPRIa (ALK-3), BMPRIb (ALK-6), and BMPRII in addition to ActRIa (ALK-2), ActRII, and ActRIIb (*22*−*24*). Since the various BMPs bind these different receptors with a broad range of affinities and specificities, this innate ability must lie in the structural differences between the BMP ligands.

BMP-6, along with BMP-5, -7, and -8, possess high affinity for their type II receptors and lower affinity for type I receptors, whereas BMP-2 or -4 exhibit higher affinity for their type I receptors (*23*, *24*). Compared to other BMPs, such as BMP-2 or BMP-7, BMP-6 has more potent osteoinducive properties as well as being shown to be the strongest inducer of human mesenchymal stem cell differentiation (*25*). BMP-6 also plays a key role in bone formation and decreased fracture healing (*26*). While BMP-6 has been shown to form complexes with a variety of receptors in different cell types (*23*), few in vitro studies have examined the structural basis of BMP-6 receptor binding affinities and comparative specificities.

Also involved in bone formation is a more distant member of the BMP family, BMP-3. BMP-3 and its closely related homologue BMP-3b (GDF-10) represent a rather distinct subgroup of BMPs, sharing only ~40% identity with other members of the BMP family ligands (*27*). Highly abundant in demineralized bone, BMP-3 was initially thought to be osteoinducive (*28*). However, recent studies have suggested that BMP-3 possesses antagonistic properties. Conditioned medium of W-20-17 cells expressing BMP-3 were shown to inhibit BMP signaling characteristics in a variety of cell types (*29*). Additionally, in *Xenopus* embryos, BMP-3 was shown to have actions opposed to those of BMP-2 (*30*). The mechanism for this unique signaling property remains unclear. Studies have proposed that BMP-3's antagonistic ability comes from its ability to signal through the Smad-2/3 (TGF-β/activin) pathway (*29*, *31*). More recently, BMP-3 was suggested to be an extracellular antagonist, similar to inhibin, by sequestering type II receptors into a nonsignaling complex (*32*). To clarify the functional mechanism of BMP-3 action, further studies with respect to structure, receptor affinity, specificity, and activity are necessary.

The current study presents two previously undetermined BMP structures, BMP-6 and BMP-3, to a resolution of 2.49 and 2.20 Å, respectively. Using known ligand−receptor complexes to generate homology models of the BMP-6 and BMP-3 structures, we identified key residues that are critically important for ligand−receptor affinity. Specifically, for BMP-3 we demonstrated how a single residue can govern specificity between different receptors and how altered receptor affinity has a direct effect on the ligand's signaling.

MATERIALS AND METHODS

Protein Expression and Purification. The mature domains of human BMP-3 (residues 1−110) and human BMP-6 (residues 1−132) were expressed in *E. coli* as inclusion bodies. The expressed inclusion bodies were isolated, purified, and refolded using a modified protocol (*33*). The refolded BMP-3 and BMP-6 were purified using a HiTrap heparin column (GE Healthcare) and reverse phase chromatography (GraceVydac). The ligands were lyophilized and resuspended in 10 mM sodium acetate, pH 4.0. The ECDs of human BMPRIa (residues 1−129) and mouse ActRIIb (residues 1−98) were expressed in *E. coli* as thioredoxin fusion proteins using a modification of published procedures (*34*). Mouse ActRII-ECD (residues 1−102) was expressed and purified from a *P. pastoris* expression system as described (*35*).

Crystallization and Data Collection. BMP-3 was crystallized using the hanging drop vapor diffusion method in 26% *tert*-butyl alcohol and 0.1 M sodium citrate, pH 5.6. The hexagonal crystals grew to an average size of 200 × 200 × 50 μm in 3 days at ambient temperature in space group *H*3 with $a = b = 96.8$ Å and $c = 101.5$ Å. The crystals were soaked in mother liquor with 15% glycerol (used as a cyroprotectant) for <5 min before being flash frozen in liquid nitrogen. Diffraction data were collected at the Advanced

Light Source (ALS) beamline 8.3.1. BMP-6 was crystallized using the hanging drop technique in 15% 2-methyl-2,4-pentanediol (MPD), 0.2 M trisodium citrate, and 0.1 M HEPES, pH 7.5. These crystals were triangular in shape and grew to 200 × 100 × 50 μm after a week at ambient temperature in space group $P3_121$ with $a = b = 97.4$ Å and $c = 87.4$ Å. The crystals were flash frozen as above with no cryoprotectant added. Diffraction data for BMP-6 were collected at the Stanford Synchrotron Radiation Laboratory (SSRL) on beamline 9-2. Both BMP-3 and BMP-6 data sets were integrated and scaled using HKL2000 (*36*). Molecular replacement, using PHASER (*37*), was used to solve for the initial phases. The best model was achieved by searching for two independent monomers in the asymmetric unit, using BMP-2 as the search model for BMP-3 and BMP-7 as the search model for BMP-6. The models were then refined using REFMAC5 (*37*) interspersed with rounds of manual building in COOT (*37*) and O (*38*). A single translation, liberation, and screw rotation (TLS) group was used for each monomer of BMP-3 and BMP-6 during the refinement. BMP-3 was refined to a final resolution of 2.20 Å with an *R* factor of 22.8% and a free *R* factor of 25.7%. BMP-6 was refined to a resolution of 2.49 Å, exhibiting an *R* factor of 23.3% and a free *R* factor of 27.6%. Both structures showed good overall geometry as determined by PROCHECK (*39*), with 89.1% and 86.4% of the residues for BMP-3 and BMP-6, respectively, in the most favored regions and none in the disallowed regions.

Surface Plasmon Resonance (BIAcore) Affinity Studies. The affinity of the ligands to BMPRIa, ActRII, and ActRIIb was monitored using a Biacore 3000 (GE Healthcare), and the data were analyzed using BIAevaluation software ver. 4.1 (GE Healthcare). Using primary amine coupling, receptor ECDs were immobilized on a CM5 chip. The receptors were immobilized independently on flow cells 2−4 for 10 min at a flow rate of 5 μL/min and a concentration of 20 μM in 10 mM sodium acetate, pH 4.0. Flow cell 1 was left blank with no immobilized protein as a negative control. The experiments were performed at a flow rate of 50 μL/min in 20 mM Tris-HCl, pH 7.9, 250 mM NaCl, 0.36% 3-[(3-cholamidopropyl)dimethylammonio]-1-propanesulfonate (CHAPS), and 0.005% Tween-20. At least five concentrations, plus a zero concentration, were used per trial for kinetic analysis, and the data were fit using a global 1:1 Langmuir binding with mass transfer. To calculate the overall K_D for each ligand, the data from all independent trials were averaged and the standard deviation was calculated as $\sigma = \sqrt{((x_i - m)^2/(n - 1))}$, where m is the mean and n is the total number of trials.

Luciferase Reporter Assays. Smad1-dependent luciferase assays were performed as previously described (*40*). In brief, C2C12 myoblast cells are cultured in Dulbecco's minimum essential medium (DMEM) + 5% FBS supplemented with L-glutamine and antibiotics. For luciferase reporter assays, cells were trypsinized, washed twice with PBS, and plated into 48-well plates with DMEM + 0.1% FBS. Twenty-four hours later, cells were transfected with −1147Id1-luciferase construct containing the Smad binding sites (Id1-Luc) (*40*, *41*), a Smad-1 expression construct, and a CAGGS-LacZ plasmid using Fugene6 (Roche) according to the manufacturer's instruction. Luciferase activity was measured 24 h after stimulation with ligands, and the values were normalized for transfection efficiency using beta-galactosidase activity. The activity of the luciferase reporter is expressed in fold induction relative to control values that are obtained using −927Id1-luciferase that lacks Smad binding domains (Id1-Luc mut).

Table 1: X-ray Collection and Data and Refinement Statistics

	BMP-3	BMP-6
data collection		
space group	*H*3	$P3_121$
no. of observations	50 312	87 590
unique reflns	17 488	16 044
resolution range (Å)[a]	28.0−2.2 (2.28−2.20)	42.5−2.49 (2.59−2.49)
average $I/\sigma I$	15.9 (6.2)	23.9 (2.0)
completeness (%)	97.9 (99.9)	93.0 (57.0)
R_{sym} (%)	5.5 (31.3)	5.3 (43.7)
refinement		
resolution range	27.96−2.20	42.5−2.49
R_{cryst} (%)	22.8	23.3
R_{free} (%)[b]	25.7	27.6
average B factor (Å^2)	46.5	63.3
rms deviation		
bonds (Å)	0.012	0.010
angles (deg)	1.327	1.396
no. of atoms		
protein	1682	1646
water	98	66
no. of TLS groups	2	2
Ramachadran analysis (non -Gly, -Pro, terminal residues)		
most favored regions	163 (89.1%)	159 (86.4%)
additionally allowed regions	16 (8.7%)	21 (11.4%)
generously allowed regions	4 (2.2%)	4 (2.2%)

[a] Numbers in parentheses correspond to the highest resolution shell. [b] Calculated from the 5% of the data not used in refinement.

RESULTS

Structure of BMP-3 and BMP-6. Table 1 summarizes the X-ray diffraction data and refinement statistics of BMP-3 and BMP-6 determined at a resolution of 2.20 and 2.49 Å, respectively. As with previously solved BMP structures, the N-terminal residues of BMP-3 (1−3) and BMP-6 (1−28) are disordered and not visible in the electron density maps. Both ligands exhibit the classic TGF-β family architecture with each monomer containing a cystine knot motif, four beta strands, and the conserved α-helix H3. Two ligand monomers are connected by an inter-subunit disulfide bond resulting in a covalently linked dimer in the overall shape of a butterfly with two curved fingers (or wings) extending outward from the cystine knot (or body) (Figure 1a for BMP-3; Figure 1b for BMP-6). Previously solved BMP complexes have shown that the type II receptors bind to the outside or knuckle region of the fingers, while the type I receptor binding site is formed by residues at the junction between two monomer subunits, near the prominent helical motif H3, designated the wrist region (*14*, *42*−*44*). The overall fold of BMP-3 is surprisingly similar to that of BMP-2, including the relative spread angle of the two wings, with an average Cα rms_{dev} of 1.02 Å over the entire molecule. The regions with the largest differences are the tip region of both fingers and the *H*3 pre-helix loop region. BMP-6 is most similar to BMP-7 with an average Cα rms_{dev} of 1.22 Å over the entire dimer. As with the structural comparison of BMP-3 and BMP-2, the *H*3 pre-helix loop region of BMP-6 (residues

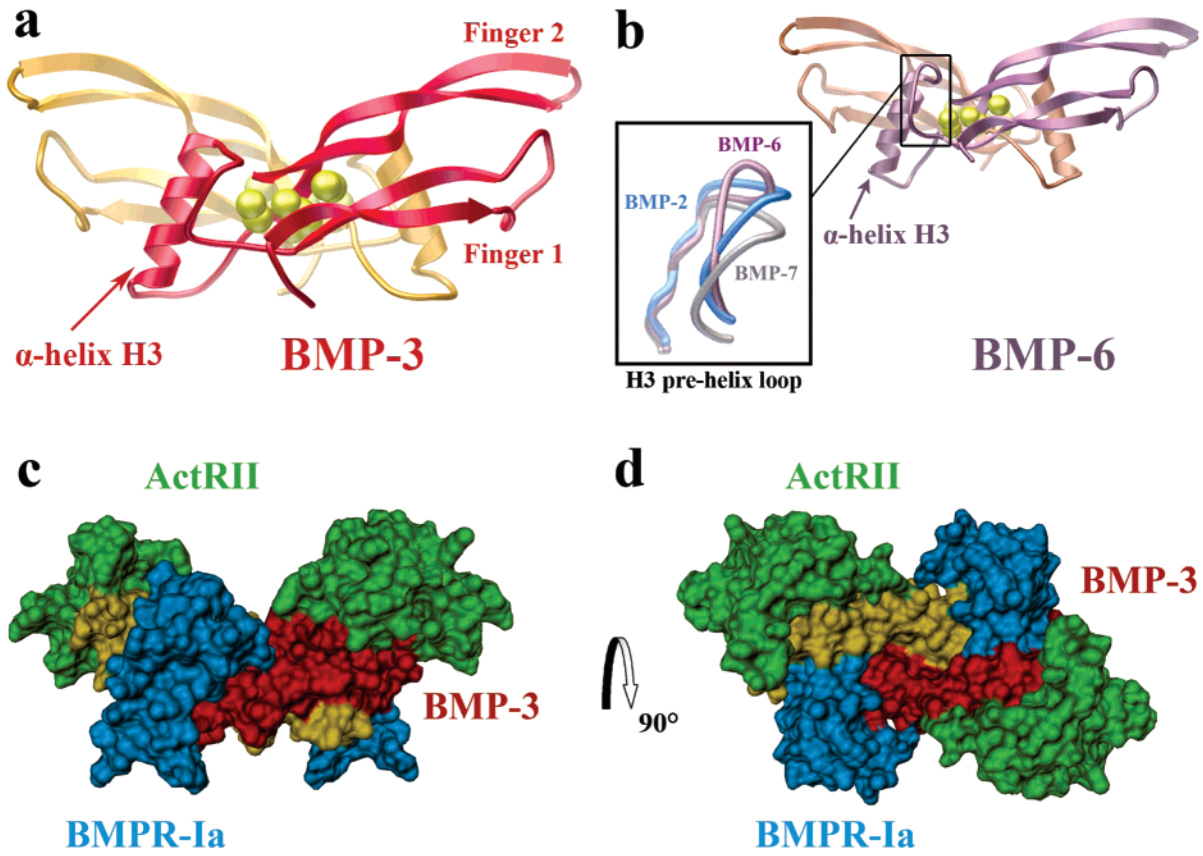

FIGURE 1: Structures BMP-3 and BMP-6 with homology model of BMP-3/BMPRIa-ECD/ActRII-ECD. (a) BMP-3 in gold and red. (b) BMP-6 in bronze and purple. Inset of b focuses on the different H3 pre-helix loop conformations of BMP-2 bound to BMPR-Ia (blue), unbound BMP-7 (gray), and unbound BMP-6 (purple). Sulfur atoms are depicted as yellow spheres. (c and d) Surface-rendered homology model of BMP-3 (red and gold) with BMPRIa-ECD (blue) and ActRII-ECD (green). Panel c is orientated as seen in the membrane, while panel d is looking down into the membrane. Panels a and b were generated using MOLSCRIPT (*63*), and panels c and d were produced using DINO (http://www.dino3d.org).

65−73) shows the largest difference between the BMP-6 and BMP-7 structures. Interestingly, this loop was observed in different conformations among noncrystallographically related monomers. In monomer B of BMP-6 (Figure 1b, bronze) the *H*3 pre-helix loop overlays very well with that of BMP-7, while in monomer A of BMP-6 (Figure 1b, purple) the loop shows a large movement, with up to a Cα rms_{dev} of 9.47 Å for residue His-71 (Figure 1b, inset). Apart from the local conformational flexibility seen in the loop regions, these results reiterate the backbone inflexibility of BMP family members as compared to activin (*13*) or TGF-*β* (*15*).

Highly Conserved Receptor-Binding Interfaces of BMP-3 and BMP-6. To delineate the structural determinants of receptor binding and specificity for BMP-3 and BMP-6, homology models were generated using the structure of the ternary complex of BMP-2/BMPRIa-ECD/ActRII-ECD as a template (*14*). The BMP-3 ligand can be superimposed over BMP-2 without significant adjustments, forming well-fit interfaces for both BMPRIa and ActRII with BMP-3. The type I interface of BMP-3 and BMPRIa is found at the junction of the BMP-3 monomers (Figure 1c,d, blue) with a predicted buried surface area of 1268 Å^2 compared to 1217 Å^2 for BMP-2:BMPRIa. The placement of the two ActRII molecules with BMP-3 (Figure 1c,d, green) gives rise to an interface similar to other previously seen type II interfaces (*13*, *14*, *42*, *44*). This is contrary to a suggestion that BMP-3 may have a unique type II binding site compared to other BMPs (*32*). The BMP-3:ActRII interface is predicted to have a buried surface area of 778 Å^2, which is slightly larger than the buried surface area of 660 Å^2 for BMP-2:ActRII and 670 Å^2 for BMP-7:ActRII. Interestingly, the recently released BMP-2:ActRIIb interface has a large buried surface area of 763 Å^2 (*43*).

As with BMP-3, BMP-6 can be readily positioned in place of BMP-2 in the ternary complex without significant adjustment to the backbone of BMP-6. The buried surface areas for BMP-6:BMPRIa (1280 Å^2) and BMP-6:ActRII (663 Å^2) compare closely with those of BMP-2:BMPRIa (1217 Å^2) and BMP-7:ActRII (670 Å^2). Interestingly, we noted that the *H*3 pre-helix loop of monomer A of BMP-6, unlike monomer B of BMP-6, is shifted dramatically away from the BMPRIa-bound conformation (modeled by BMP-2:BMPRIa structure, Figure 1b inset, blue). If the *H*3 pre-helix loop of monomer A remained in this position (Figure 1b inset, purple), the side chains of these residues would sterically clash with residues from BMPRIa. To avoid these potential clashes, the apparently flexible *H*3 pre-helix loop of BMP-6 must adopt a conformation closer to that of the bound BMP-2 upon binding BMPRIa. The predicted ternary complexes of both BMP-3 and BMP-6 display different receptor types that would not contact each other (Figure 1 c,d).

A detailed comparison of the contacts formed at the interfaces of BMP-3:ActRII, BMP-3:ActRIIb (based on homology model to the activin:ActRIIb structure (*13*)), and

BMP-6:ActRII (based on the homology model to the BMP-7:ActRII structure (*42*)) strengthens the hypothesis of a common binding mode for all type II interfaces. The hydrophobic core contacts, as well the most highly conserved contacts seen in previously solved type II interfaces, are predicted in all three new interfaces (Figure 2b−d, pink and green residues). Similar to previously solved ligand−receptor complexes, the majority of the unique residue contacts are located at the periphery of the binding interfaces (Figure 2b−d, blue residues). Further, the contacts in the predicted BMP-3:ActRII interface closely resemble the contacts in the recently published BMP-2:ActRIIb interface (Figure 2e). Minor differences in the contact residues between the BMP-3 type II interfaces are probably due to slight positional changes between the residues of ActRII and ActRIIb and the experimental cutoff distance of 4 Å for contacts. For instance, although residues Lys-37 and Asn-65 are present and positionally equivalent in both ActRII and ActRIIb, they are only noted in the BMP-3:ActRII interface in Figure 2 because of the aforementioned criteria.

BMP-3 Preferentially Binds ActRIIb. The highly conserved structural framework among BMP−receptor interfaces suggests that ligand−receptor affinity and specificity is encoded by a few key amino acids. While previous studies have shown that BMP-3 is capable of binding ActRIIb (*32*) and that BMP-3 can antagonize the actions of BMP-2 (*31*, *32*), the nature of these BMP-3−receptor interactions have been poorly characterized. Using surface plasmon resonance (BIAcore) we measured the binding affinities of BMP-3 to ActRII-ECD and BMPRIa-ECD by individually immobilizing the receptor ECDs to the chip surface. BMP-3_{wt} binds to BMPRIa-ECD and ActRII-ECD with affinities of K_d = 0.307 and 1.84 μM, respectively (Table 2), suggesting that both BMPRIa and ActRII are relatively low-affinity receptors for BMP-3. A typical high-affinity receptor interaction for BMP ligands shows a K_d of 1−5 nM, while lower affinity receptor interactions are typically found in the 50−200 nM range. Binding affinities are shown for BMP-2 and BMP-7 tested on the same chip surface for comparison (Table 2). In contrast to the very low affinity of BMP-3_{wt} to ActRII-ECD ($K_d \approx 1.8$ μM), the affinity of BMP-3_{wt} to ActRIIb-ECD is K_d = 52.6 nM (Table 2). This is a surprising 30-fold higher affinity as compared to ActRII-ECD and also 6-fold higher affinity than compared to BMPRIa-ECD (K_d = 307 nM), indicating that ActRIIb is the true higher affinity receptor for BMP-3. Because all other ligands we tested do not show such a high degree of discrimination between ActRII and ActRIIb, these results indicate a unique ability of BMP-3 in encoding its type II receptor specificity.

Closer comparison of the two predicted BMP-3 type II interfaces with known type II interfaces yielded two key amino acids, Ser-28 and Asp-33, that are uniquely present in BMP-3. Ser-28 of BMP-3 lies at the bottom of the hydrophobic core of the interface, packing against Phe-83 of ActRII (Figure 3, box 1). The polar side chain of Ser-28 presents a potential steric hindrance as well as an unfavorable interaction with the nonpolar surface of the receptor. Disruption to this hydrophobic core has been previously shown to inhibit binding of ActRII (*45*). Sequence comparison with all other BMP sequences shows that BMP-3 is the only ligand to have a serine at this location, whereas all other ligands have an alanine. The second amino acid, Asp-33,

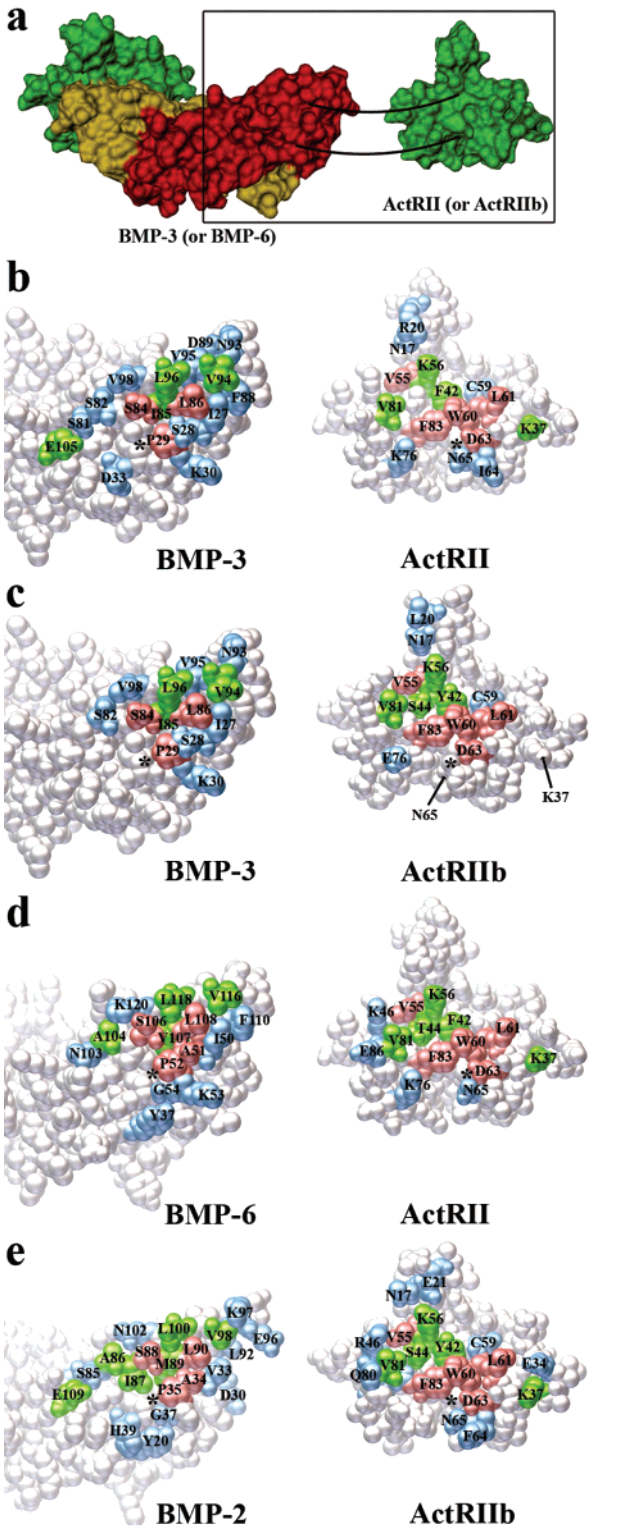

FIGURE 2: Predicted type II interfaces of BMP-3 and BMP-6 with ActRII or ActRIIb. (a) Surface rendering of a BMP ligand with a type II receptor peeled away, and the box highlights the close-up region for panels b−e. Panels b−e represent the type II interfaces as space-filling models. (b) BMP-3:ActRII interface, and (c) BMP-3:ActRIIb interface. (d) BMP-6:ActRII interface. (e) Recently solved BMP-2:ActRIIb interface as comparison. The asterisks in panels b−e represent interface contact points. Identical contacts, compared with known interfaces of BMP-2:ActRII, BMP-7:ActRII, and activin:ActRIIb, are shown in pink, and highly conserved contacts are shown in green. Unique contacts are shown in blue. Panel a was produced using DINO (http://www.dino3d.org), while panels b−e were generated using MOLSCRIPT (*63*).

Table 2: Ligand Affinity Data from BIAcore Experiments[a]

ligand	BMP-2	BMP-6	BMP-7	BMP-3_{wt}	BMP-3_{S28A}	BMP-3_{D33A}
			receptor BMPRIa			
k_{off} [1/s]	$1.85 \times 10^{-3} \pm 1.7 \times 10^{-4}$	$1.06 \times 10^{-2} \pm 1.2 \times 10^{-3}$	$7.21 \times 10^{-2} \pm 1.6 \times 10^{-3}$	$5.18 \times 10^{-2} \pm 2.3 \times 10^{-3}$	no data	no data
k_{on} [1/M·s]	$7.06 \times 10^{5} \pm 1.6 \times 10^{4}$	$1.58 \times 10^{5} \pm 8.0 \times 10^{3}$	$4.33 \times 10^{4} \pm 8.0 \times 10^{3}$	$1.69 \times 10^{5} \pm 3.0 \times 10^{3}$		
K_D [nM]	2.61 ± 0.18	67.2 ± 4.4	1680 ± 145	307 ± 19		
			receptor ActRII			
k_{off} [1/s]	$7.65 \times 10^{-2} \pm 8.6 \times 10^{-3}$	$3.54 \times 10^{-3} \pm 1.7 \times 10^{-3}$	$1.19 \times 10^{-2} \pm 4.0 \times 10^{-4}$	$1.78 \times 10^{-1} \pm 2.6 \times 10^{-2}$	$7.71 \times 10^{-2} \pm 5.4 \times 10^{-3}$	$1.73 \times 10^{-1} \pm 5.8 \times 10^{-2}$
k_{on} [1/M·s]	$1.60 \times 10^{6} \pm 3.0 \times 10^{4}$	$4.60 \times 10^{5} \pm 1.9 \times 10^{5}$	$3.44 \times 10^{6} \pm 4.1 \times 10^{5}$	$9.91 \times 10^{4} \pm 2.4 \times 10^{4}$	$8.13 \times 10^{5} \pm 1.3 \times 10^{5}$	$1.34 \times 10^{6} \pm 2.8 \times 10^{5}$
K_D [nM]	47.5 ± 6.5	7.39 ± 0.71	3.49 ± 0.30	1840 ± 180	96.5 ± 9.5	124 ± 16
			receptor ActRIIb			
k_{off} [1/s]	$4.34 \times 10^{-2} \pm 7.0 \times 10^{-4}$	$6.32 \times 10^{-3} \pm 1.2 \times 10^{-3}$	$1.67 \times 10^{-2} \pm 1.1 \times 10^{-3}$	$6.82 \times 10^{-2} \pm 1.7 \times 10^{-2}$	$4.36 \times 10^{-3} \pm 9.8 \times 10^{-4}$	$5.39 \times 10^{-3} \pm 1.5 \times 10^{-3}$
k_{on} [1/M·s]	$1.18 \times 10^{6} \pm 8.0 \times 10^{4}$	$9.17 \times 10^{5} \pm 3.8 \times 10^{4}$	$2.14 \times 10^{6} \pm 2.0 \times 10^{4}$	$1.29 \times 10^{6} \pm 2.7 \times 10^{5}$	$3.91 \times 10^{5} \pm 7.0 \times 10^{3}$	$1.41 \times 10^{5} \pm 1.2 \times 10^{5}$
K_D [nM]	36.1 ± 1.3	6.87 ± 1.0	7.72 ± 0.53	52.6 ± 2.0	11.3 ± 2.8	4.06 ± 1.48
			receptor $ActRIIb_{E76K}$			
k_{off} [1/s]	$3.59 \times 10^{-2} \pm 9.0 \times 10^{-3}$	no data	no data	no data	$4.11 \times 10^{-2} \pm 2.0 \times 10^{-3}$	no data
k_{on} [1/M·s]	$6.98 \times 10^{5} \pm 8.0 \times 10^{4}$				$3.02 \times 10^{5} \pm 1.9 \times 10^{4}$	
K_D [nM]	50.3 ± 6.6				137 ± 15	

[a] The BIAcore data is shown as the dissociation rate, k_{off}, and the association rate, k_{on}, based on a global fit using the kinetic model 1:1 Langmuir binding with mass transfer. The binding constant K_D is calculated as k_{off}/k_{on}. The table reports data from a single trial. No data indicates that the interaction was not measured. The receptors were immobilized to the chip surface with the ligands flowed over the surface.

FIGURE 3: Ribbon diagram highlighting the key residues of the type II interface between ActRII and BMP-3. Box 1 shows how the Phe-83 of ActRII (green) is predicted to pack against the wild-type Ser-28 of BMP-3 in yellow and the mutated Ala-28 in gray. Box 2 depicts the proposed interaction between Ile-64 of ActRII with wild-type Asp-33 of BMP-3 (red and yellow) and the mutant Ala-33 in gray. Box 3 depicts Lys-30 of BMP-3 interacting with Glu-76 (gray) and then mutation to Lys-76 (green) of ActRIIb. Sulfur atoms in BMP-3 are shown as yellow spheres. This figure was made using MOLSCRIPT (*63*).

lies near the periphery of the interface and is predicted to interact with Ile-64 of ActRII (Figure 3, box 2). As with Ser-28, Asp-33 presents potential stereochemical and charge barriers to binding. When these two potentially unfavorable interactions were removed by individually mutating the residues to alanine, both BMP-3_{S28A} and BMP-3_{D33A} mutants showed a 20-fold increase in affinity for ActRII-ECD compared to BMP-3_{wt} (Table 2). Furthermore, BMP-3_{S28A} and BMP-3_{D33A} also show a 10- and 20-fold increase in affinity to ActRIIb-ECD (Table 2). The K_d of BMP-3_{S28A} and BMP-3_{D33A} to ActRIIb-ECD is 11.3 and 4.06 nM, respectively, making them near-high- to high-affinity interactions. A double mutant of BMP-$3_{S28A/D33A}$ does not show a further increase in binding affinity over the single mutants, indicating that their contributions to the binding energy are highly coupled because of the proximity between them.

BMP-3 and BMP-6 Receptor Specificity. While the BMP-3_{S28A} and BMP-3_{D33A} mutants account for a significant increase in overall affinity to both ActRII and ActRIIb by removing their potentially unfavorable interactions at the type II receptor-binding interface, the specificity determinant for the 30-fold affinity difference of BMP-3 between ActRII and ActRIIb must be encoded on the receptor. Among residues at the interface of BMP-3 with either ActRII or ActRIIb, Lys-76 of ActRII and Glu-76 of ActRIIb are unique such that they are positioned to form either an unfavorable or favorable interaction with Lys-30 of BMP-3 (Figure 3, box 3). To test the idea that Lys-30 is one of the key residues encoding the specificity between ActRII and ActRIIb, a mutation of Glu-76 to Lys-76 was introduced into ActRIIb. By removing the favorable charge interaction present between Lys-30 of BMP-3 and Glu-76 of ActRIIb, ActRIIb now mimics ActRII. For this experiment, BMP-3_{S28A}, a high-affinity ligand to ActRII-ECD, was used to compare its affinity more readily to ActRIIb-ECD_{E76K}. Compared to ActRIIb-ECD, the affinity of BMP-3_{S28A} to ActRIIb-ECD_{E76K} was decreased 10-fold from K_d = 11.3 to 137 nM (Table

2). This new affinity was comparable, if not weaker, than the affinity to ActRII-ECD (K_d = 96.5 nM). BMP-2 has a proline at the position structurally equivalent to Lys-30 of BMP-3 and does not exhibit a difference in affinity between ActRIIb-ECD and ActRIIb-ECD$_{E76K}$ (Table 2).

The high degree of discrimination in affinity between ActRII and ActRIIb appears to be unique to BMP-3. BMP-2, BMP-6, BMP-7, and activin do not display a significant discrimination for their type II receptors. For instance, BMP-6 shows comparable affinities of K_d = 7.39 and 6.87 nM for ActRII-ECD and ActRIIb-ECD, respectively (Table 2). BMP-7 also displays similar type II receptor affinities to those of BMP-6 (Table 2), which would be expected from their high degree of similarity. While BMP-6 and BMP-7 share similar biological functions and type II receptor affinities, it is interesting to note the large difference in type I receptor affinity. The affinity of BMP-7 to BMPRIa-ECD at K_d = 1.67 μM is over 20-fold weaker than the affinity of BMP-6 to BMPRIa-ECD with a K_d = 67.2 nM (Table 2). Initial comparisons of the type I interfaces of BMP-6 and BMP-7 with BMPRIa-ECD have yet to identify single, key residues responsible for this affinity difference (data not shown). This result indicates that type I receptor affinity may be mediated through the arrangement of multiple residues rather than individual residues as seen in the type II interfaces.

BMP-3 Mutants Can Activate the Smad-1/5/8 Pathway. To test whether the receptor affinity data are relevant to the functional activity of BMP-3, we made use of a luciferase reporter system that illustrates TGF-β signaling activities quantitatively. To characterize the interactions of BMP-3 and BMP-6 with the receptors BMPR-Ia, ActRII, and ActRIIb, we chose the Id1-Luc as a reporter clone. It is known that BMP receptors signal through the Smad-1/5/8 pathway and the Id1 promoter contains a well-characterized Smad-1-binding site responding to activated Smad-1 (*46*). Removal of this site (Id1-Luc mut) abolishes any response, demonstrating that the Id1-Luc is a Smad-1-dependent reporter (*40*). The C2C12 cell line was chosen as it expresses numerous BMP-specific receptors including Alk-2 (ActRIa), Alk-3 (BMPRIa), Alk-6 (BMPRIb), BMPRII, and ActRII (*23*, *47*−*49*). Additional TGF-β receptors Alk-4 (ActRIb), Alk-5 (TGF-βRI), Alk-7, and TGF-βRII are also expressed in this cell line (*47*, *49*). Even in the studies designed to detect ActRIIb, ActRIIb expression was not found in C2C12 cells (*47*, *49*). The absence of ActRIIb in C2C12 cells has been confirmed in our own experiments (data not shown). Because fetal bovine serum (FBS) is known to contain BMP-like activity (*41*), we used low serum concentration, 0.1% FBS, in order to minimize any interference on the assay.

We first compared signaling activities of the wild-type ligands. As reported previously, BMP-2 shows strong signaling activity in a concentration-dependent manner (Figure 4a). This is consistent with our and others' (*50*) data showing high affinity of BMP-2 to BMPRIa-ECD (Table 2). BMP-7 also displayed strong stimulation of the Smad-1-dependent pathway, similar to BMP-2. Despite its relatively low affinity to BMPRIa, BMP-7 is still able to signal because C2C12 cells express ALK-2 which can activate Smad-1 (*51*). BMP-6 shows weak signaling activity with only 2.3- and 9.01-fold Id1-Luc stimulation at 10 and 100 ng/mL, respectively. This stimulation is approximately 8−13% of the Id1-Luc activation by the same concentration of BMP-2 (Figure 4a). BMP-3 showed an insignificant and nonconcentration-dependent level of signaling through the Smad-1 pathway (Figure 4a). BMP-3's poor receptor affinity most likely accounts for this observed inability to signal. To test if higher receptor affinity impacts ligand activity, we compared the activity of the BMP-3 mutant ligands in the Smad-1-dependent reporter assay. The BMP-3$_{S28A}$ mutant showed a significant increase in its ability to activate the Id1-Luc reporter and stimulated the reporter activity 13.7-fold at 300 ng/mL (Figure 4b). Introduction of the S28A mutation now increases BMP-3 activity to a level similar to that of BMP-6. Interestingly, although BMP-3$_{D33A}$ has similar affinity for ActRII-ECD as BMP-3$_{S28A}$, BMP-3$_{D33A}$ did not exhibit as significant an activation of the Id1-Luc reporter as did BMP-3$_{S28A}$ with only a 3.2-fold stimulation at 300 ng/mL (Figure 4b).

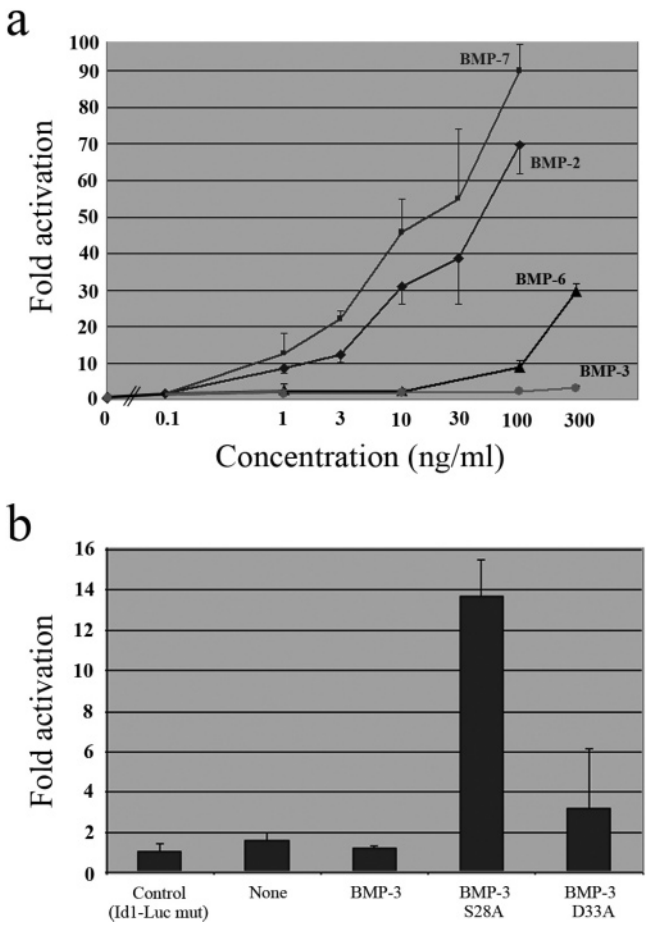

FIGURE 4: Smad-1 luciferase reporter assays display various BMP ligand activities. (a) Activities of BMP-2, BMP-3, BMP-6, and BMP-7 as an increase in relative fold activity over background. (b) Activities of BMP-3$_{wt}$, BMP-3$_{S28A}$, and BMP-3$_{D33A}$ as relative fold increases in activity above background. For both graphs, fold activation values are mean ± standard deviation from triplicated experiments, the *x* axis shows the ligand concentration in ng/mL, while the *y* axis shows the relative fold activity.

DISCUSSION

How the approximately 40 TGF-β superfamily ligands differentially bind and signal through only 12 common receptors remains elusive. The disparity in the number of receptors to ligands means each receptor has multiple ligand binding partners. For instance, ActRII binds activin and BMP-7 with high affinity, around 1 nM, while binding

BMP-2 with lower affinity at ~50 nM (Table 2) (*14*, *42*). We and others have previously shown that a hydrophobic core is highly conserved between both lower and high-affinity type II interfaces (*14*, *44*). On the basis of our newly solved crystal structures of BMP-3 and BMP-6, their predicted type II interfaces with ActRII or ActRIIb also share this motif (Figure 2b−d). Using BIAcore with immobilized receptor ECDs, BMP-6 bound ActRII-ECD with high affinity, similar to BMP-7, while BMP-3 displayed extremely low affinity at ~2 μM. (Table 2). A closer look at the predicted BMP-3:ActRII interface revealed residues Ser-28 and Asp-33 in BMP-3 to be unique compared other known type II interfaces. Mutation of either residue to alanine to remove unfavorable interactions resulted in an increase in affinity to ActRII-ECD of 20-fold. Both of these residues are found in the loop region of finger 1 in BMP-3 and suggest this loop plays a major role in determining type II receptor affinity. Interestingly, residues at the top of the hydrophobic core have been shown to affect type II binding in other TGF-β ligands. In activin, mutation of Lys-102 has been shown to decrease binding to ActRII (*52*), while in BMP-2 a single mutant L100K (*14*) (equivalent to Lys-102 in activin) or double mutant L100K/N102D (*44*) has been shown to increase BMP-2 binding to ActRII or ActRIIb, respectively.

Our data shows that BMP-3 binds ActRIIb-ECD with 30-fold higher affinity than to ActRII-ECD (Table 2). This large difference in affinity of BMP-3 to ActRIIb over ActRII is surprising given that the ECDs of ActRII and ActRIIb are 63% identical and 92% similar. Further, the buried surface area of the BMP-3:ActRII interface is predicted to be much larger than the BMP-3:ActRIIb interface. However, buried surface area for the type II interface does not seem to dominate overall affinity. For example, BMP-2 has similar affinity for ActRII-ECD and ActRIIb-ECD, but the BMP-2:ActRIIb interface has 15% more buried surface area. Among those ActRII binding ligands we studied, activin shows the next largest difference in affinity, only 4-fold, between these receptors. Even though the BMP-3_{S28A} and BMP-3_{D33A} mutations increased overall affinity to both ActRII-ECD and ActRIIb-ECD, they did not account for the affinity difference between the receptors. Comparison of the BMP-3:ActRII and BMP-3:ActRIIb interfaces yielded one significant difference: Lys-30 of BMP-3 makes a potentially favorable interaction with Glu-76 of ActRIIb, which is structurally equivalent to Lys-76 of ActRII. When the E76K mutation was introduced into ActRIIb, BMP-3 affinity could indeed be decreased for ActRIIb-ECD to the level of ActRII-ECD (Table 2). This suggests that BMP-3 type II receptor specificity is largely controlled by a single amino acid contact through Lys-30. This single amino acid specificity switch has been seen in other TGF-β ligands. For instance, a single amino acid in GDF-5 was shown to regulate type I receptor specificity (*53*), while a three amino acid group in the different TGF-β isoforms determines affinity to TGF-βRII (*54*). This general notion that a single residue or a few residues dominate receptor binding affinity has also been demonstrated in other systems, such as human growth hormone receptor binding (*55*).

Previous studies failed to show activity using recombinant BMP-3, and these results may have simply been due to the poor affinity of BMP-3 for ActRII. To test if the higher affinity of the BMP-3 mutants correlates to higher signaling activity, we compared their activity against wild-type BMP-3 activity in C2C12 cells. Consistent with previous results, BMP-3_{wt} did not show significant activity; however, the BMP-3_{S28A} mutant showed comparable activity to that of BMP-6 (Figure 4a and b). This is similar to a report in which increased affinity of BMP-2 to ActRIIb results in increased activity in C2C12 cells (*44*). Even though BMP-3_{D33A} displayed a similar increase in affinity for ActRII-ECD as BMP-3_{S28A}, it failed to show a comparable increase in activity in our luciferase assays. The inability of BMP-3_{D33A} to increase cellular signaling activity despite its increased binding affinity to ActRII-ECD highlights the complexity of the signaling in a cell. This discrepancy between the mutants may be explained by influences of other components in the ligand−receptor assembly occurring on the cell surface for productive signaling. Our data shows that higher affinity of the BMP-3 mutants to isolated ActRII-ECD, as demonstrated on the BIAcore chip surface, is a reasonable but not an entirely accurate predictor for increased signaling activity. This apparent disjunction between affinity and activity is not unprecedented in other systems (*56*). We predict that BMP-3_{wt} will signal through ActRIIb in a similar manner to BMP-3_{S28A} with ActRII because they share comparable receptor binding affinities. The lack of activity of BMP-3_{wt} in our assays is due to the absence of ActRIIb expression in C2C12 cells, which has been previously reported (*23*, *47*−*49*).

BMP-3 was shown to complex with ActRIIb and ALK-4 (*32*), which is similar to the activin signaling complex known to signal through the Smad-2/3 pathway (*51*). It has been suggested that BMP-3, by signaling through the Smad-2/3 pathway, could antagonize BMP-2 function intracellularily (*31*). Therefore, how BMP-3_{wt} can function as a BMP antagonist while the BMP-3_{S28A} mutant can activate the Smad-1/5/8 pathway remains unclear. One potential key may be the prodomain of BMP-3. It has been shown that BMP prodomains can regulate signaling activity, stability, and signaling range of the mature domains (*57*, *58*). Much of the functional work with BMP-3 has been performed using conditioned medium containing BMP-3. This medium may contain the prodomain as well as the mature domain of BMP-3, which could alter BMP-3's function if the two domains interact. In the case of BMP-9 crystallized from conditioned medium, the prodomain was shown to be present and form a tight noncovalent complex with the mature BMP-9 dimer (*59*). The prodomains of numerous other BMP ligands have also been shown to noncovalently bind the mature ligand as well as other proteins in the extracellular matrix (*60*, *61*). Another possible regulation mode for BMP-3 could be the presence of unknown co-receptors on the cell surface. Cripto and Betaglycan are known TGF-β ligand co-receptors important for modulating receptor binding and signaling (*22*). The binding of BMP-3 to either one of these molecules, or a similar molecule, might affect downstream signaling. Finally, we cannot exclude the possibility that the binding of BMP-3 to different type II receptors (ActRII vs ActRIIb) may alter type I receptor recruitment. These differences in final complex formation may result in changes to downstream signaling.

Although highly homologous, BMP-6 and BMP-7 appear to have distinct type I receptor specificities with BMP-6 displaying a 20-fold higher affinity to BMPRIa-ECD than BMP-7 but 20-fold lower than BMP-2 (Table 2). This result

was unexpected because BMP-6 shares numerous receptor binding and signaling characteristics with BMP-7 (*23*, *62*). The inability to obtain active BMP-7 in large yields has limited its structural and functional studies, but now with the structure of BMP-6 and the ability to alter its receptor binding properties, a better understanding of the determinants of low-affinity type I binding is attainable. Comparison of the BMP-6 structure to the structures of BMP-7 and BMP-2 should be instrumental in identifying the residues responsible for these differences in affinity. Experiments with BMP-6, as well as focusing on a binary structure with type I receptors, will yield greater understanding of overall receptor binding.

The ultimate transmembrane signaling mechanism executed by TGF-β ligand is complex. However, our data demonstrates that one or a few specific amino acid residues of BMP-3 can govern receptor interactions. This provides us with the basis to stipulate that specific amino acid residue differences at the ligand−receptor binding interfaces are the pivotal components in regulating receptor affinity and defining a ligand's signaling activity. BMP ligands, in particular, are multifunctional signaling molecules that act in a variety of biological processes. Our report highlights the possibility that ligands and secreted antagonists can be engineered for the purpose of targeting receptors that are not reachable by natural ligands. Such engineered molecules will be instrumental to develop future controlled applications such as for stem cell maintenance and modulation of stem cell differentiation pathways.

ACKNOWLEDGMENT

We would like to thank the staff of the Stanford Synchrotron Radiation Laboratory and the Advanced Light Source, especially James Holton, beamline 8.3.1, for his excellent technical assistance with X-ray data collection, Mark Vega for numerous discussions, Robert Benezra for the Id1-luciferase reporters, Henry Juguilon for excellent technical assistance, and Elizabeth Komives for BIAcore data collection.

NOTE ADDED AFTER ASAP PUBLICATION

This paper was published on October 9, 2007 with a typographical error in the Results section. The corrected version was published on October 12, 2007.

SUPPORTING INFORMATION AVAILABLE

Representative BIAcore traces for BMP-3 and BMP-6. This material is available free of charge via the Internet at http://pubs.acs.org.

REFERENCES

1. Massagué, J., Blain, S. W., and Lo, R. S. (2000) TGF-β Signaling in Growth Control, Cancer, and Heritable Disorders, *Cell 103*, 295−309.
2. Sun, L. (2004) Tumor-suppressive and promoting function of transforming growth factor beta, *Front. Biosci.* 11.
3. Waite, K. A., and Eng, C. (2003) From Developmental Disorder to Heritable Cancer: It's all in the BMP/TGF-beta Family, *Nat. Rev. Genet. 4*, 763−773.
4. Cutroneo, K. R. (2003) Gene therapy for tissue regeneration, *J. Cell Biochem. 88*, 418−425.
5. Valdimarsdottir, G., and Mummery, C. (2005) Functions of the TGF-beta superfamily in human embryonic stem cells, *APMIS 113*, 773−789.
6. Cui, Y., Hackenmiller, R., Berg, L., Jean, F., Nakayama, T., Thomas, G., and Christian, J. L. (2001) The activity and signaling range of mature BMP-4 is regulated by sequential cleavage at two sites within the prodomain of the precursor, *Genes Dev. 15*, 2797−2802.
7. McDonald, N. Q., and Hendrickson, W. A. (1993) A structural superfamily of growth factors containing a cystine knot motif, *Cell 73*, 421−424.
8. Liao, W. X., Moore, R. K., Otsuka, F., and Shimasaki, S. (2003) Effect of Intracellular Interactions on the Processing and Secretion of Bone Morphogenetic Protein-15 (BMP-15) and Growth and Differentiation Factor-9. Implication of the Aberrant Ovarian Pheotype of BMP-15 Mutant Sheep, *J. Biol. Chem. 278*, 3713−3719.
9. Israel, D. I., Nove, J., Kerns, K. M., Kaufman, R. J., Rosen, V., Cox, K. A., and Wozney, J. (1996) Heterodimeric bone morphogenetic proteins show enhanced activity *in vitro* and *in vivo*, *Growth Factors 13*, 10.
10. Keah, H. H., and Hearn, M. T. W. (2005) A molecular recognition paradigm: promiscuity associated with the ligand-receptor interactions of the activin members of the TGF-beta superfamily, *J. Mol. Recognit. 18*, 385−403.
11. Greenwald, J., Fischer, W. H., Vale, W. W., and Choe, S. (1999) Three-finger toxin fold for the extracellular ligand-binding domain of the type II activin receptor serine kinase, *Nat. Struct. Mol. Biol. 6*, 18−22.
12. Nishitoh, H., Ichijo, H., Kimura, M., Matsumoto, T., Makishima, F., Yamaguchi, A., Yamashita, H., Enomoto, S., and Miyazono, K. (1996) Identification of Type I and Type II Serine/Threonine Kinase Receptors for Growth/Differentiation Factor-5, *J. Cell Biochem. 271*, 21345−21352.
13. Greenwald, J., Vega, M. E., Allendorph, G. P., Fischer, W. H., Vale, W., and Choe, S. (2004) A Flexible Activin Explains the Membrane-Dependent Cooperative Assembly of TGF-β Family Receptors, *Mol. Cell 15*, 485−489.
14. Allendorph, G. P., Vale, W. W., and Choe, S. (2006) Structure of the ternary signaling complex of a TGF-beta superfamily member, *Proc. Natl. Acad. Sci. 103*, 7643−7648.
15. Hart, P. J., Deep, S., Taylor, A. B., Shu, Z., Hinck, C. S., and Hinck, A. P. (2002) Crystal structure of the human TβR2 ectodomain-TGF-β3 complex, *Nat. Struct. Mol. Biol. 9*, 203−208.
16. Laiho, M., Weis, M. B., and Massagué, J. (1990) Concomitant loss of transforming growth factor (TGF)-beta receptor types I and II in TGF-beta-resistant cell mutants implicates both receptor types in signal transduction, *J. Biol. Chem. 265*, 18518−18524.
17. Attisano, L., and Wrana, J. L. (1996) Signal transduction by members of the transforming growth factor-β superfamily, *Cytokine Growth Factor Rev. 7*, 327−339.
18. Shi, Y., and Massagué, J. (2003) Mechanisms of TGF-β Signaling from Cell Membrane to the Nucleus, *Cell 113*, 685−700.
19. Miyazono, K. (2000) Positive and negative regulation of TGF-beta signaling, *J. Cell Sci. 113*, 1101−1109.
20. Urist, M. R. (1965) Bone: Formation by Autoinduction, *Science 150*, 893−899.
21. Morrison, S. J., Shah, N. M., and Anderson, D. J. (1997) Regulatory Mechanisms in Stem Cell Biology, *Cell 88*, 287−298.
22. Harrison, C. A., Wiater, E., Gray, P. C., Greenwald, J., Choe, S., and Vale, W. (2004) Modulation of activin and BMP signaling, *Mol. Cell. Endocrinol. 225*, 19−24.
23. Ebisawa, T., Tada, K., Kitajima, I., Tojo, K., Sampath, T. K., Kawabata, M., Miyazono, K., and Imamura, T. (1999) Characterization of bone morphogenetic protein-6 signaling pathways in osteoblast differentiation, *J. Cell Sci. 112*, 3519−3527.
24. Yamashita, H., Ten Dijke, P., Heldin, C. H., and Miyazono, K. (1996) Bone morphogenetic protein receptors, *Bone 19*, 569−574.
25. Friedman, M. S., Long, M. W., and Hankenson, K. D. (2006) Osteogenic differentiation of human mesenchymal stem cells is regulated by bone morphogenetic protein-6, *J. Cell Biochem. 98*, 538−554.
26. Kugimiya, F., Kawaguchi, H., Kamekura, S., Chikuda, H., Ohba, S., Yano, F., Ogata, N., Katagiri, T., Harada, Y., Azuma, Y., Nakamura, K., and Chung, U.-i. (2005) Involvement of Endogenous Bone Morphogenetic Protein (BMP) 2 and BMP6 in Bone Formation, *J. Biol. Chem. 280*, 35704−35712.
27. Takao, M., Hino, J., Takeshita, N., Konno, Y., Nishizawa, T., Matsuo, H., and Kangawa, K. (1996) Identification of Rat Bone

Morphogenetic Protein-3b (BMP-3b), a New Member of BMP-3, *Biochem. Biophys. Res. Commun. 219*, 656−662.
28. Wozney, J. M., Rosen, V., Celeste, A. J., Mitsock, L. M., Whitters, M. J., Kriz, R. W., Hewick, R. M., and Wang, E. A. (1988) Novel regulators of bone formation: molecular clones and activities, *Science 242*, 1528−1534.
29. Bahamonde, M. E., and Lyons, K. M. (2001) BMP3: To Be or Not To Be a BMP, *J. Bone Joint Surg. Am. 83*, S56−62.
30. Hino, J., Nishimatsu, S.-i., Nagai, T., Matsuo, H., Kangawa, K., and Nohno, T. (2003) Coordination of BMP-3b and cerberus is required for head formation of Xenopus embryos, *Dev. Biol. 260*, 138−157.
31. Daluiski, A., Engstrand, T., Bahamonde, M. E., Gamer, L. W., Agius, E., Stevenson, S. L., Cox, K., Rosen, V., and Lyons, K. M. (2001) Bone morphogenetic protein-3 is a negative regulator of bone density, *Nat. Genet. 27*, 84−88.
32. Gamer, L. W., Nove, J., Levin, M., and Rosen, V. (2005) BMP-3 is a novel inhibitor of both activin and BMP-4 signaling in Xenopus embryos, *Dev. Biol. 285*, 156−168.
33. Groppe, J., Rumpel, K., Economides, A. N., Stahl, N., Sebald, W., and Affolter, M. (1998) Biochemical and Biophysical Characterization of Refolded Drosophila DPP, a Homolog of Bone Morphogenetic Proteins 2 and 4, *J. Biol. Chem. 273*, 29052−29065.
34. Kirsch, T., Nickel, J., and Sebald, W. (2000) Isolation of recombinant BMP receptor IA ectodomain and its 2:1 complex with BMP-2, *FEBS Lett. 468*, 215−219.
35. Greenwald, J., Le, V., Corrigan, A., Fischer, W., Komives, E., Vale, W., and Choe, S. (1998) Characterization of the Extracellular Ligand-Binding Domain of the Type II Activin Receptor, *Biochemistry 37*, 16711−16718.
36. Otwinowski, Z., and Minor, W. (1997) *Processing of X-ray Diffraction Data Collected in Oscillation Mode*, Vol. 276, Academic Press.
37. Collaborative Computational Project, N. (1994) The CCP4 suite: programs for protein crystallography, *Acta Crystallogr., Sect. D* 760−763.
38. Jones, T. A., Zou, J. Y., Cowan, S. W., and Kjeldgaard, M. (1991) Improved methods for building protein models in electron density maps and the location of errors in these models, *Acta Crystallogr., Sect. A* 110−119.
39. Laskowski, R. A., MacArthur, M. W., Moss, D. S., and Thornton, J. M. (1993) PROCHECK: a program to check the stereochemical quality of protein structures, *J. Appl. Crystallogr.* 283−291.
40. Nakashima, K., Takizawa, T., Ochiai, W., Yanagisawa, M., Hisatsune, T., Nakafuku, M., Miyazono, K., Kishimoto, T., Kageyama, R., and Taga, T. (2001) BMP2-mediated alteration in the developmental pathway of fetal mouse brain cells from neurogenesis to astrocytogenesis, *Proc. Natl. Acad. Sci. 98*, 5868−5873.
41. Suzuki, A., Raya, A., Kawakami, Y., Morita, M., Matsui, T., Nakashima, K., Gage, F. H., Rodriguez-Esteban, C., and Izpisua Belmonte, J. C. (2006) Nanog binds to Smad1 and blocks bone morphogenetic protein-induced differentiation of embryonic stem cells, *Proc. Natl. Acad. Sci. 103*, 10294−10299.
42. Greenwald, J., Groppe, J., Gray, P., Wiater, E., Kwiatkowski, W., Vale, W., and Choe, S. (2003) The BMP7/ActRII Extracellular Domain Complex Provides New Insights into the Cooperative Nature of Receptor Assembly, *Mol. Cell 11*, 605−617.
43. Kirsch, T., Sebald, W., and Dreyer, M. K. (2000) Crystal structure of the BMP-2-BRIA ectodomain complex, *Nat. Struct. Mol. Biol. 7*, 492−496.
44. Weber, D., Kotzsch, A., Nickel, J., Harth, S., Seher, A., Mueller, U., Sebald, W., and Mueller, T. D. (2007) A silent H-bond can be mutationally activated for high-affinity interaction of BMP-2 and activin type IIB receptor, *BMC Struct. Biol. 7*, 6.
45. Gray, P. C., Greenwald, J., Blount, A. L., Kunitake, K. S., Donaldson, C. J., Choe, S., and Vale, W. (2000) Identification of a Binding Site on the Type II Activin Receptor for Activin and Inhibin, *J. Biol. Chem. 275*, 3206−3212.
46. Lopez-Rovira, T., Chalaux, E., Massagué, J., Rosa, J. L., and Ventura, F. (2002) Direct Binding of Smad1 and Smad4 to Two Distinct Motifs Mediates Bone Morphogenetic Protein-specific Transcriptional Activation of Id1 Gene, *J. Biol. Chem. 277*, 3176−3185.
47. Yeh, L.-C. C., Tsai, A. D., Zavala, M. C., and Lee, J. C. (2004) Cartilage-derived morphogenetic proteins enhance the osteogenic protein-1-induced osteoblastic cell differentiation of C2C12 cells, *J. Cell. Phys. 201*, 401−408.
48. Namiki, M., Akiyama, S., Katagiri, T., Suzuki, A., Ueno, N., Yamaji, N., Rosen, V., Wozney, J. M., and Suda, T. (1997) A Kinase Domain-truncated Type I Receptor Blocks Bone Morphogenetic Protein-2-induced Signal Transduction in C2C12 Myoblasts, *J. Biol. Chem. 272*, 22046−22052.
49. De Jong, D. S., Van Zoelen, E. J. J., Bauerschmidt, S., Olijve, W., and Steegenga, W. T. (2002) Microarray Analysis of Bone Morphogenetic Protein, Transforming Growth Factor beta, and Activin Early Response Genes During Osteoblastic Cell Differentiation, *JBMR 17*, 2119−2129.
50. Keller, S., Nickel, J., Zhang, J.-L., Sebald, W., and Mueller, T. D. (2004) Molecular recognition of BMP-2 and BMP receptor IA, *Nat. Struct. Mol. Biol. 11*, 481−488.
51. Feng, X.-H., and Derynck, R. (2005) Specificity and Versatility in TGF-beta signaling through Smads *Annu. Rev. Cell Dev. Biol. 21*, 659−693.
52. Wuytens, G., Verschueren, K., de Winter, J. P., Gajendran, N., Beek, L., Devos, K., Bosman, F., de Waele, P., Andries, M., van den Eijnden-van Raaij, A. J. M., Smith, J. C., and Huylebroeck, D. (1999) Identification of Two Amino Acids in Activin A That Are Important for Biological Activity and Binding to the Activin Type II Receptors, *J. Biol. Chem. 274*, 9821−9827.
53. Nickel, J., Kotzsch, A., Sebald, W., and Mueller, T. D. (2005) A Single Residue of GDF-5 Defines Binding Specificity to BMP Receptor IB, *J. Mol. Biol. 349*, 933−947.
54. De Crescenzo, G., Hinck, C. S., Shu, Z., Zuniga, J., Yang, J., Tang, Y., Baardsnes, J., Mendoza, V., Sun, L., Lopez-Casillas, F., O'Connor-McCourt, M., and Hinck, A. P. (2006) Three Key Residues Underlie the Differential Affinity of the TGF-β Isoforms for the TGF-β Type II Receptor, *J. Mol. Biol. 355*, 47−62.
55. Pal, G., Ultsch, M. H., Clark, K. P., Currell, B., Kossiakoff, A. A., and Sidhu, S. S. (2005) Intramolecular Cooperativity in a Protein Binding Site Assessed by Combinatorial Shotgun Scanning Mutagenesis, *J. Mol. Biol. 347*, 489−494.
56. Wilmen, A., Pick, H., Niedenthal, R. K., Sen-Gupta, M., and Hegemann, J. H. (1994) The yeast centromere CDEI/Cpf1 complex: differences between in vitro binding and in vivo function, *Nucl. Acids Res. 22*, 2791−2800.
57. Constam, D. B., and Robertson, E. J. (1999) Regulation of Bone Morphogenetic Protein Activity by Pro Domains and Proprotein Convertases, *J. Biol. Chem. 144*, 139−149.
58. Le Good, J. A., Joubin, K., Giraldez, A. J., Ben-Haim, N., Beck, S., Chen, Y., Schier, A. F., and Constam, D. B. (2005) Nodal Stability Determines Signaling Range, *Curr. Biol. 15*, 31−36.
59. Brown, M. A., Zhao, Q., Baker, K. A., Naik, C., Chen, C., Pukac, L., Singh, M., Tsareva, T., Parice, Y., Mahoney, A., Roschke, V., Sanyal, I., and Choe, S. (2005) Crystal Structure of BMP-9 and Functional Interactions with Pro-region and Receptors, *J. Biol. Chem. 280*, 25111−25118.
60. Sopory, S., Nelsen, S. M., Degnin, C., Wong, C., and Christian, J. L. (2006) Regulation of Bone Morphogenetic Protein-4 Activity by Sequence Elements within the Prodomain, *J. Biol. Chem. 281*, 34021−34031.
61. Jasuja, R., Ge, G., Voss, N. G., Lyman-Gingerich, J., Branam, A. M., Pelegri, F. J., and Greenspan, D. S. (2007) Bone Morphogenetic Protein 1 Prodomain Specifically Binds and Regulates Signaling by Bone Morphogenetic Proteins 2 and 4, *J. Biol. Chem. 282*, 9053−9062.
62. Solloway, M. J., Dudley, A. T., Bikoff, E. K., Lyons, K. M., Hogan, B. L. M., and Robertson, E. J. (1998) Mice lacking *Bmp6* function, *Dev. Genet. 22*, 321−339.
63. Kraulis, P. (1991) MOLSCRIPT: a program to produce both detailed and schematic plots of protein structures, in Journal of Applied Crystallography. *Appl. Crystallogr.* 946−950.

BI700907K